SciMedCentral

JSM Nanotechnology & Nanomedicine

Review Article

Interface Modifications of Porous Silicon for Chemical Sensor Applications

Caitlin Baker and James L. Gole*

School of Physics, Georgia Institute of Technology, USA

Corresponding author

James L Gole, School of Physics, Georgia Institute of Technology, 837 State Street, Atlanta, GA, 30332-0430, USA, Tel: 404-894-4029; E-mail: James.Gole@physics.gatech.edu

Submitted: 11 March 2014

Accepted: 28 May 2014

Published: 29 May 2014

Keywords

- Photochemical smog
- Asthma
- CO_2
- $NH_3(PH_3)$
- Volatile organic compounds

Abstract

We present a review/perspective on current developments in nanostructure modified porous silicon (PS) interfaces for reversible chemical gas sensing. Detection levels and mechanisms associated with different sensor designs are evaluated and discussed. In part, the focus will be on recent enhancements of organic molecule detection through optical and capacitance sensors. New fabrication methods address past issues of repeatability and we consider the stabilization of PS structures by various oxidation and carbonation methods. We discuss the detection of inorganics facilitated using polymer films and nanostructure deposition. A major focus is on nanostructure-modified nanopore coated microporous porous silicon sensors as well as the effect and applications of in-situ modification of the nanostructures. This combination of studies from the past five years provides the possibility of a sensitive and selective array of PS gas sensors.

ABBREVIATIONS

PS: Porous Silicon; **FWHM:** Full Width Half Maximum; **RIE:** Reactive Ion Etching; **SOI:** Silicon on Insulator; **DMF:** Dimethyl Formamide; **TEOS:** Tetraethoxysilane; **PPy:** Polypyrolle; **SEM:** Scanning Electron Microscopy; **PECVD:** Plasma-Enhanced Chemical Vapor Deposition; **TBAP:** Tetra Butyl Ammonium Perchlorate; **MeCN:** Acetonitrile; **IHSAB:** Inverse Hard/Soft Acid/Bases; **HSAB:** Hard/Soft Acid/Base; **HOMO:** Highest Occupied Molecular Orbital; **LUMO:** Lowest occupied Molecular Orbital.

INTRODUCTION

Porous silicon (PS) has attracted attention for gas sensing due to the unique combination of advantageous properties [1]. In this review, recent chemical sensing applications will be discussed. Electrochemically fabricated by anodic etching in an HF solution, PS features high surface area, luminescence properties, and ease of integration with microelectronic devices. By adjusting the etch parameters, the morphology, pore size, and porosity can be changed and reasonably controlled [2].

There is an increasing demand for sensitive and selective gas sensing with applications in toxic gas detection and manufacturing process monitoring [3]. NO_x is a toxic gas associated with air pollution, combustion and respiratory disease [3,4]. Exhaled nitric oxide is correlated with asthmatic conditions such as airway inflammation and with the potential to provide rapidly accessed noninvasive disease detection [5]. An asthmatic attack produces large quantities of NO, which can combine with O_2 to produce NO_2. In addition, NH_3 emissions have been detected, however at a much lower level than are typically associated with urban environments [6,7]. Monitoring of automotive and industrial combustion exhaust, responsible for acid rain, photochemical smog, and corrosion, involves the detection of NO_x and SO_2 [3]. There is also an increasing demand for the detection of fuel combustion products CO (toxic and odorless) and CO_2 (a global warming factor) [3]. PH_3, an extremely toxic gas, is used in agriculture for fumigation and is a byproduct in the production of methamphetamines [8,9]. Detection of volatile organic vapors is necessary for personal protective equipment [10] and as a means of assessing the outgassing of the solvents associated with building materials and indoor furnishings [11].

Differentiation between atmosphere or combustion gases has been approached by developing an array of selective sensors. Jalkanen et al. accomplish this by simultaneous monitoring of two selective properties of PS (optical and capacitance) in response to organic vapors [12]. Gole et al. are developing an array of metal oxide nanostructure modified PS sensors with a range of selectivities to various inorganic and select organic molecules [13]. This review/perspective discusses the current PS gas sensor designs enhancing sensitivity and selectivity with a focus to the use of detection interfaces that represent a minimum health hazard. At present the inherent sensitivity for inorganic species greatly exceeds that for organic constituents.

POROUS SILICON CHEMICAL GAS SENSORS

Organic Detection

The dielectric function of PS, as it is sensitive to organic

vapors, allows for sensing through capacitance and optical measurements [14,1]. Jalkanen et al. have developed a PS gas sensor by monitoring the capacitance and reflectance changes of the PS in response to ambient adsorbates [12]. By monitoring multiple parameters, selectivity between vapors can be enhanced. PS sensors were formed by anodizing a p+-type silicon wafer (0.01-0.02 Ω-cm) in a 1:1 HF/ethanol solution. PS with a stop band in the infrared range was formed by modulating the etching current between 10 and 100 mA/cm^2 with a 20 s period. By changing the current density, the porosity concentration can be controlled allowing the creation of layers of different reflectivity [15]. The PS sensor was then stabilized to a hydrophobic surface by carbonation below 600 °C to create a humidity resistant sensor. A hydrophilic surface, for a sensor sensitive to humidity changes, is created by carbonation above 680 °C [12,15]. Carbonation is required to prevent the natural oxidation of the anodized PS.

The optical properties of the PS sensors are observed using an InGaAs-photodetector once IR radiation is introduced via a bifurcated optical fiber. Vapor concentration is observed as a redshift in reflected IR radiation. Acetone, decane, DMF, methylamine, and toluene induced a linear redshift as a function of adsorbate concentration. In contrast, the redshift grew exponentially with hexane concentration [15], as shown in (Figure 1). By way of future comparison, it is to be noted that a change of 1% in hexane concentration corresponds to 10,000 ppm. Jalkanen et al. observed a correlation between redshift and the saturated vapor pressure value of the adsorbates.

The shape of the spectra was also slightly altered in response to the various vapors. The full width at half maximum (FWHM) of the spectra was measured to compare the degree of spectral shape alteration with acetone, decane, and methylamine having the strongest effect [15]. While is it normal for the FWHM value to increase with a redshift in the spectra, the FWHM change due to the organic vapors was greater than expected, in the case of acetone, or inverse of expected, in the case of decane. Instead, adsorbate affinity to PS layers with different indexes of refraction, related to porosity, is a possible reason for the FWHM change [15]. Jalkanen et al. propose the vapor induced spectral alterations as a parameter to differentiate between adsorbate effects and obtain selectivity for optical sensor responses. Selectivity of the optical sensors to acetone and methylamine is illustrated in (Figure 2) by analyzing both the redshift and spectral shape change.

Nguyen et al. have improved detection of D-(+)-glucose and Cy5-conjugated Rabbit Anti-Mouse IgG by fabricating a PS sensor with cascaded nano-porous layers [16]. Nano-porous layers were created by electrochemical etching of p- and n-type silicon wafers (0.001-0.005 Ω) in 15% HF in ethanol with a 3 electrode configuration. The silicon wafers were set as the working electrode and the reference and counter electrodes were Pt. Alternating current densities formed the cascading porous silicon layers. The p-type silicon sensors featured 20 alternating layers of porosity 25% (40 mA/cm^2) and 40% (60 mA/cm^2) with a defect layer of 60% (80 mA/cm^2). Similarly, the n-type silicon sensors featured alternating layers of porosity 69% (40 mA/cm^2) and 58% (34 mA/cm^2) with a defect layer of 69% (40 mA/cm^2) [16]. Samples were subsequently oxidized at 500 °C to maintain a stable and hydrophilic porous surface.

Mid-IR FTIR spectra were collected of the PS sensor under DI water and a range of diluted D-(+)-glucose and Cy5-conjugated Rabbit Anti-Mouse IgG samples [16]. The sensitivity to D-(+)-glucose was a redshift of 50 cm^{-1}/mM with a limit of detection calculated to be 80 μM. The sensitivity to Cy5-conjugated Rabbit Anti-Mouse IgG was a redshift of 96 cm^{-1}/μM with a limit of detection of 40 nM. The cascaded nano-porous layers of the PS sensor improve the detection by a factor of 2.8 for D-(+)-glucose and by a factor of 2.5×10^5 for Cy5-conjugated Rabbit Anti-Mouse IgG [16].

The elegant method of reflectance monitoring involves challenges including reproducibility due to imprecise positioning of optical fibers. To improve reproducibility of the monitoring of optical property changes, Karcali et al. have developed a fabrication process to integrate a fiber optic cable directly into the bulk Si [14]. The new design features more robust reflectivity measurements by eliminating measurement error from variation in fiber optic cable alignment angle, shortening experiment set-up time, and allowing for flexible positioning of the sensor. The first fabrication step involves hole milling by reactive ion etching (RIE) of the insulator backside of a silicon on insulator (SOI) wafer. A thin oxide layer between the silicon and insulator is used to reliably stop the RIE process [14]. The porous layer is formed by electrochemical anodic etching in a 1:2 HF (40%) and ethanol (95%) solution. The etching current density is set to 600 mA/cm^2 for 120s to thin the silicon layer by electro-polishing. The current density is then adjusted linearly from 100 mA/cm^2 for 10s, to create an index profile to suppress undesired reflections. This is followed by 876.8 s of sinusoidally modulated current of 19 – 21 mA/cm^2 to fabricate the detection multilayers. A final linear change from 20 mA/cm^2 to 200 μA/cm^2 again eliminates unwanted reflections. The fiber optic cable is then integrated into the PS sensor by fixing with epoxy at an optimized position [14]. The authors admit that this new design necessitates a "thorough and methodological preparation" [14].

PS sensor device optical measurements were compared for ethanol, methanol, propanol, and butanol [14]. The measurements from the integrated PS sensor had a lower variance for all vapors. The integrated PS sensor as opposed to a conventional PS sensor was able to differentiate between the

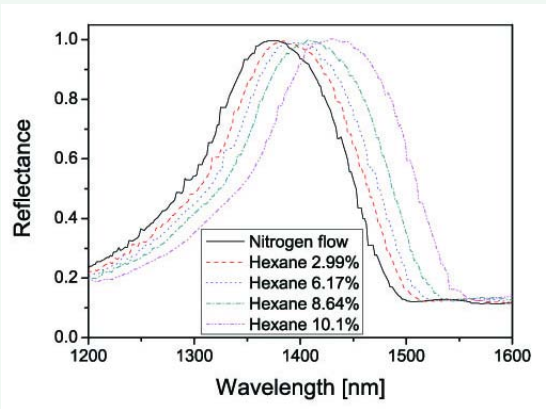

Figure 1 Redshift induced by hexane vapor adsorption to porous silicon [15].

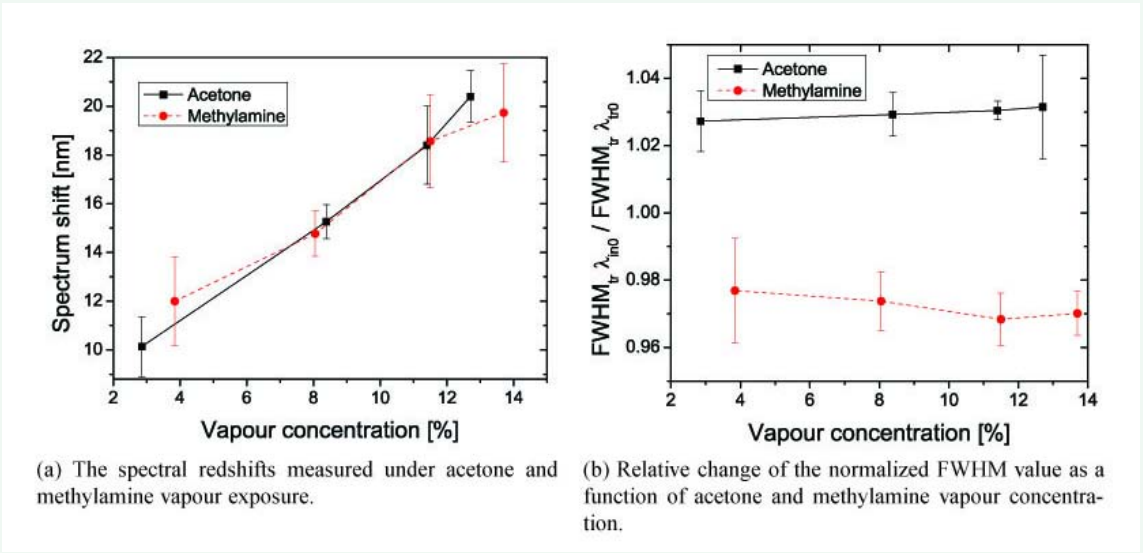

(a) The spectral redshifts measured under acetone and methylamine vapour exposure.

(b) Relative change of the normalized FWHM value as a function of acetone and methylamine vapour concentration.

Figure 2 Comparison of redshift and FWHM spectral change of optical response to acetone and methylamine [15].

reflectivity wavelengths shifts from 1-propanol and 2-propanol. However, the conventional PS sensor could differentiate between 1-butanol and 2-butanol where the integrated PS sensor could not [14].

The combination of optical measurements and capacitance is monitored to enhance selectivity for vapor detection [12]. Jalkanen et al. deposited 20 nm thick gold electrodes by argon plasma sputtering and recorded capacitance with an LCR meter. Capacitance changes were measured in response to ethanol and DMF vapor. As expected, the hydrophilic PS sensor was unaffected by changes in humidity. Selectivity was displayed by plotting both the capacitance and reflectance change against the relative pressure of the organic vapors (Figure 3). Optimization of optical response and capacitance response require opposite changes in PS morphology and so the combined application of these methods can be complex. Jalkanen et al. therefore recommended an array of sensors optimized to individual detection methods [12].

Alternatively, it may be possible to improve sensitivity by conforming detection to a low temperature entrainment/conductometric detection platform. Here, we employ a double slush-bath configuration using dry ice and hexanol. With these slush baths, we create a cooled nitrogen flow in a bubble flow configuration to entrain toluene. The toluene is separately cooled to a vapor pressure producing an effective concentration between 10 and 100 ppm. The nitrogen and toluene are cooled by separate and complimentary hexanol/dry ice slush baths whose temperatures are adjusted between -50 and -60 C. The entrained toluene is found to produce a detectable signal corresponding to several ohms.

Sol-gel synthesis with PS sensors can enhance selectivity to acetone vapor. Moshnikov et al. used a sol-gel process [17] to deposit metal oxide nanomaterials to electrically anodized n-type porous silicon. Inorganic salts of iron, nickel, tin and cobalt were added to tetraethoxysilane (TEOS). Hydrolysis and polycondensation of the TEOS solution was performed to obtain the metal oxide materials with the ability to form a *film* to spread

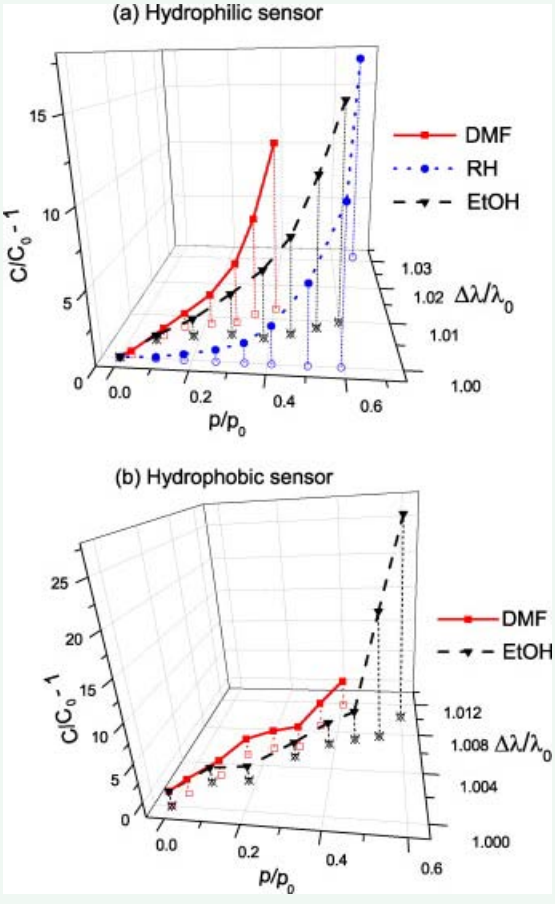

Figure 3 Differentiation between DMF and ethanol by plotting capacitance and optical response of (a) hydrophilic and (b) hydrophobic PS sensors [12].

Reprinted from Sensors and Actuators B: Chemical, 147, TeroJalkanen, JaaniTuura, ErmeiMäkilä, JarnoSalonen, Electro-optical porous silicon gas sensor with enhanced selectivity, 100-104, Copyright (2010), with permission from Elsevier.

over the PS [17]. They collected impedance spectra of the PS/metal oxide sensor in response to acetone vapor to measure the increase in sensitivity due to the deposition. The calculated resistance of the PS sensor decreased in response to the vapor and the maximum relaxation frequency increased by a factor of 2 – 7 depending on the metal oxide deposition [17].

Liyanage and Blackwood have achieved selectivity between ethanol and acetone by attaching functional organic groups onto a porous silicon impedance sensor [18]. The PS was formed by electrochemical etch in a 1:2:1 solution of HF, ethanol, and deionized water for 20 min with a current density of 22 mA/cm^2 under backside 200 W halogen illumination. After freeze-drying to prevent cracking, the PS was functionalized with either 1-decene or undecylenic acid. The functionalization method involved exposing the PS to a heated mixture of paraffin oil and organic molecules for 24 hours. The paraffin was then removed by immersion in pentane for 1 hour [18].

While the impedance of the PS sensor decreases with increasing ethanol or acetone concentration, the linearity of the response reveals selectivity. The sensor functionalized with 1-decane displays a linear response increase for both analytes. However, the undecylenic acid functionalized sensor does not produce a continuous linear response. The authors suggested that this is due to a difference of interactions available to the functionalized surfaces. The 1-decane treated surface can only undergo weak van der Waals interaction, but the undecylenic acid can undergo strong H-bonding. Additionally, the undecylenic acid interacts more strongly with ethanol than acetone leading to the different linear response pattern of the two analytes [18].

Hu et al fabricated a PS/CdTenanocrystal composite humidity sensor that features selectivity against common volatile organic compounds [19]. To create the composite, the PS layer was first silanized with (3-aminopropyl) triethoxysilane and then immersed in diluted HCl, which protonated the amino group. A CdTenanocrystal solution, dripped on the layer, diffused across the protonated-silanized PS. Hu et al found that the presence of water vapor decreased the amount of photoradiation surface traps, increasing the photoluminescence of the composite sensor surface. The linear detection range was found to be 12% to 93% relative humidity concentrations and, with the exception of a very weak signal for NH_3 [19], no detectable signals were obtained from common volatile organic compounds at concentrations of 26.4 µg/mL.

Cho et al. observed the simultaneous detection of organic gasses as well as the pressure from measuring the optical properties of rugate-structured porous silicon [20]. They noted that while organic vapors, in this case 6000 ppm of IPA, produce a red-shift of the reflectance peak as discussed earlier, the peak intensity decreased with lowering pressure. However, the authors note a mutual interference of the responses [20].

Inorganic detection

Conductometric PS sensors are sensitive to resistance changes as a function of gas analyte concentration. Gole and Ozdemir describe [21] the changes in the extrinsic semiconductor charge carrier populations that occur in the presence of inorganic gas analytes. An analyte acting as a Lewis base can donate electrons to the PS interface. For p-type PS, the majority charge carriers, electron holes, combine with the donated electrons and are reduced in number therefore increasing the resistance of the PS. In contrast, for n-type PS, the majority charge carriers are electrons and so the electron transfer from analytes increases the majority charge carrier population, thus decreasing the resistance [21].

Tebizi-Teighilt et al. formed polypyrrole *films* on porous silicon by cyclic voltammetry to create a PS sensor which they suggest is sensitive to CO_2 [22]. P-type silicon wafers were electrochemically etched in 1:1 HF/ethanol solution for 5 min at a current density of 10 mA/cm^2 and then stabilized with an ozone treatment for 10 min. A 1 µm layer of polypyrolle (PPy) was deposited by electrochemical polymerization. The PPy was found to be poorly adherent to the PS and storage and drying increased the fragility of the structures. However, after the PS was oxidized by ozone exposure the structure was stabilized and the PPy coating strongly adhered to the surface [22].

The CO_2 sensing capabilities of the PPy/oxide PS sensors were tested by measuring the current-voltage characteristics for a range of bias voltages (-1 V to +2 V) [22]. In the presence of 500 ppm of CO_2 gas, the sensor displayed a decrease of dc current with a maximum sensitivity at 0.45 V bias voltage for the oxided PS sensor and 1 V for the PS sensor. As shown in (Figure 4), the response to CO_2 for both PPy/PS and PPy/oxide PS is instantaneous with a rapid current recovery time of about 2 min. Tebizi-Teighilt et al. suggest that the sensing interaction mechanism is due to CO_2 molecules forming weak bonds with the pi-electrons of the PPy and is enhanced over polypyrrole sensors by the high surface area of the PS and oxided PS and adsorption into the pores of these adsorbates [22].

Yan et al. have studied room temperature detection of NO_2 by measuring the resistance across sensors with a programmable professional digital multimeter [23]. The PS sensors were exposed to various concentrations of gas by injecting the analyte gas into an enclosed chamber. The porous silicon was fabricated

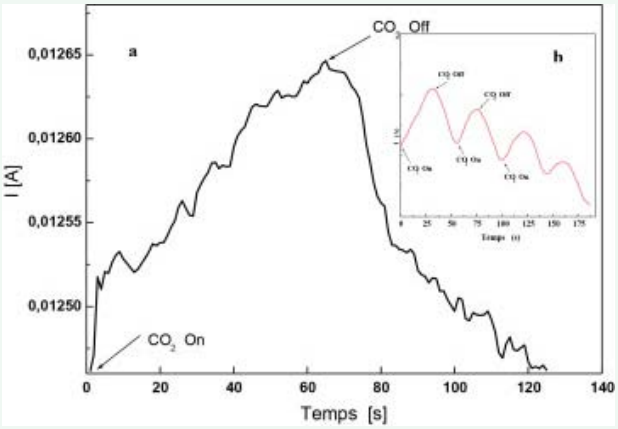

Figure 4 (a) Response of PPy/PS and (b) PPy/oxide PS to CO_2 gas [22].

Reprinted from Applied Surface Science, 269, Fatma-ZohraTebizi-Tighilt, Fawzi Zane, Naima Belhaneche-Bensemra, Samia Belhousse, Sabrina Sam, and Nour-EddineGabouze, Electrochemical gas sensors based on polypyrrole-porous silicon, 180-183, Copyright (2013), with permission from Elsevier.

by a double cell anodic etching of p-type silicon wafers in a 1:2 HF and DMF solution with a current density of 100 mA/cm^2. Pt electrodes 100 nm thick were deposited onto the PS surface by RF magnetron sputtering [23]. The final sensor measured 4 mm x 16 mm with two 3 mm x 3 mm Pt electrodes. Detection of NO_2 was enhanced by ZnO electrochemical deposition. The deposited ZnO nanostructures formed were characterized by SEM showing that nanosheets, nanorods, or dendritic nanostructures of ZnO were formed on the surface of the PS layer (Figure 5) depending on the pH value of the electrochemical solution [23]. The resistance change response of the PS/ZnO sensors was compared showing the samples with ZnO nanosheets to have the greatest increase in sensitivity and the sample with dendritic ZnO to have almost the same sensitivity as PS [23]. Yan et al. propose that the reason for the better gas sensing properties of the nanosheets is due to either possible higher surface area or a more apparent interface effect between the nanosheets and PS since the thickness of the sheets is much smaller than the diameter of the nanorods [23]. Additionally, the ZnO nanostructured PS sensors exhibited a high selectivity to NO_2 over NH_3, H_2S, and organic vapors [23].

Tungsten oxide nanowires also appear to enhance the response to NO_2 [24]. Ma et al. prepared PS/WO_3 nanostructured sensors by first coating PS with a thin film of tungsten by magnetron sputtering. Tungsten is deposited up to 150 nm thick on PS, and then forms nanowires by annealing under oxygen and argon at temperatures of 600-750 °C for 1 h (Figure 6). The resistance change of the PS/WO_3 nanowire sensor was measured in response to 2ppm of NO_2, 50 ppm NH_3, and 100 ppm of ethanol and acetone. The sensor showed selectivity to NO_2 with a relative response change of 4.76 at an optimal testing temperature of 150 °C analogous to traditional metal oxide devices. The sensor response to the other gas analytes was negligible [24]. Similarly, the PS response to NO_2 was enhanced by the addition of TeO_2 nanowires [25]. Tellurium powder was thermally evaporated onto the PS sample for 2 hours at 400 °C. The response (change in resistance) of the PS/TeO_2 sensor to 1 ppm of NO_2 was approximately 5.7 times the response of blank PS [25]. This result demonstrates the potential for signal improvement with the proper deposition of nanostructured metal oxides but the use of TeO_2 and the complexity of the approach used to prepare the surface do not justify its use over similarly sensitive surfaces.

Nanopore coated microporous PS interfaces have been created to detect low ppm levels of NH_3, NO_x, CO, SO_2 and PH_3 [26,27]. These are rapidly responding, reversible, and sensitive sensors, which operate at *room temperature*. Selectivity to different gas analytes has been established with the deposition of select nanoparticles. These nanoparticles direct a reversible electron transduction, predicted by the now developing IHSAB principle [13]. The metal oxide nanoparticles are amenable to in-situ modification, thus extending the range of selective responses and providing additional applications through the modification of the metal oxide nanostructures at the PS gas sensor interface.

The PS sensor interface can be created using either n- or p-type silicon wafers. An insulating SiC mask layer is deposited by plasma-enhanced chemical vapor deposition (PECVD) and etched to reveal 2 mm x 5 mm windows to the silicon surface by reactive ion etching (RIE). The revealed silicon is then etched by electrochemical anodization. For the n-type, a 1:1

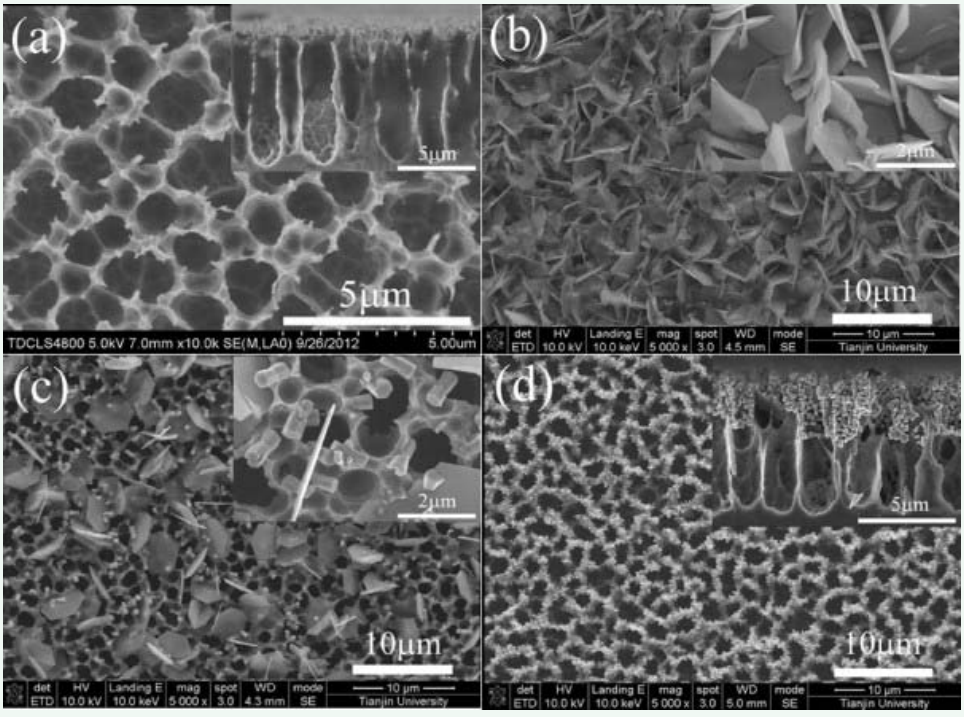

Figure 5 SEM images of (a) PS, (b) ZnOnanosheets , (c) ZnOnanorods, and (d) dendridicZnO formed on PS [23].

Reprinted from ElectrochimicaActa, 115, Dali Yan,Ming Hu,Shenyu Li,Jiran Liang,Yaqiao Wu, and Shuangyun Ma, Electrochemical deposition of ZnO nanostructures onto porous silicon and their enhanced gas sensing to NO2at room temperature, 297-305, Copyright (2014), with permission from Elsevier.

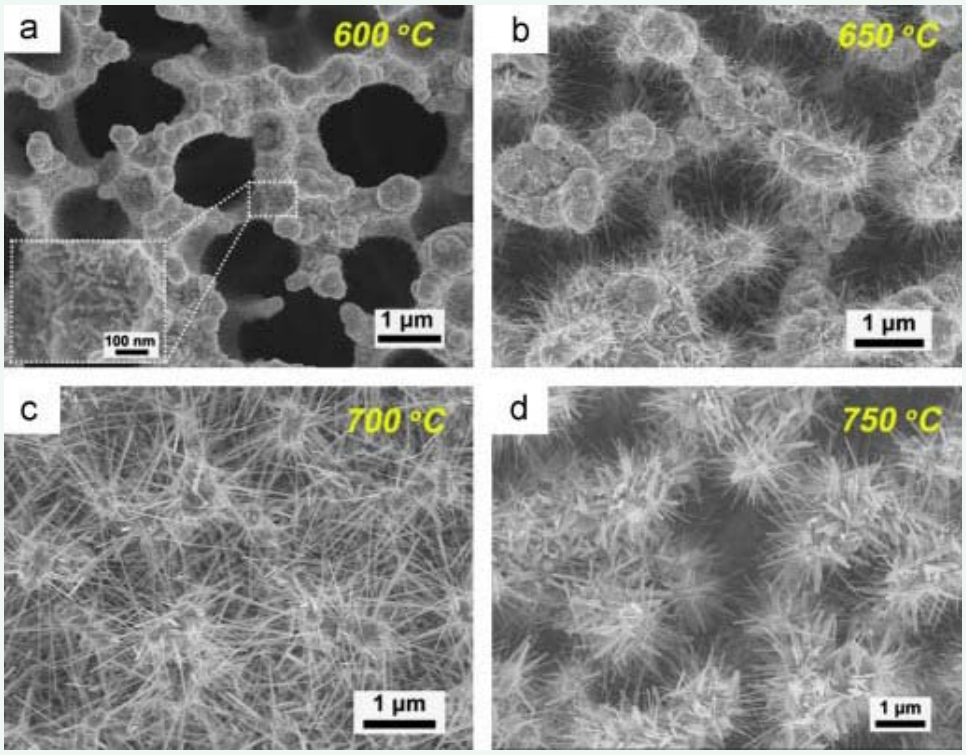

Figure 6 SEM images of tungsten nanowires formed on PS after annealing for 1 h at (a) 600 °C, (b) 650 °C, (c) 700 °C, and (d) 750 °C [24].

Reprinted with permission from (Ma S, Hu M, Zeng P, Li M, Yan W, Li C. Synthesis of tungsten oxide nanowires/porous silicon composites and their application in NO2 sensors. Materials Letters. 2013; 112: 12-15.). Copyright (2013) American Chemical Society.

solution of HF and ethanol is used under front side UV radiation (Blak-Ray Hg Lamp) with a current density of 14 mA/cm^2. The resultant PS feature pore diameters of 0.5-0.7 µm with typical depths of 50-75 µm. P-type wafers are etched with a solution of 0.1 M tetrabutylammonium perchlorate (TBAP) and 1 M HF in acetonitrile (MeCN) with a current density of 3 mA/cm^2 [13]. This etch procedure creates an array of micropores, 0.8-1.5 µm in diameter, with nanopore coated walls. Etch duration determines the micropore depth ~10-30 µm. Electrical contacts formed from 10 nm of titanium followed by 200 nm of gold are deposited by electron beam evaporation. (Figure 7) shows a schematic of the sensor design and the configuration of the gas sensor setup. A fabricated wafer is diced to create 12 individual sensors [13].

As demonstrated in (Figure 8), the detection of low ppm concentrations of gas analytes is rapid and reversible. The system is operated at 1-3 V range with an extremely low power requirement [4]. In contrast to traditional metal oxide sensors the PS sensor can be operated in a modified heat sunk configuration. The sensor is placed on a copper block, which is in intimate contact with a temperature controlled heating element. This heating element is adjusted in temperature from 25 to 240 °C, producing temperatures ranging from 25 to 75 °C (Figure 8). In other words the sensors can be readily heat sunk and the degree of heat sinking increases with temperature. Since the heat sinking is created in a solid-on-solid interface environment it represents a lower bound to the temperature range that can be accommodated in a gas-on solid environment. In particular, the sensor can distinguish between concentrations in the low ppm concentration for a range of temperatures extending to at least 75 °C (Figure 8). Calculations would suggest that the heat sinking in this environment will operate at considerably higher gas temperatures. Operation in a 500 °C diffuse gas flow is not unrealistic. The signal to noise can be improved at the elevated temperatures by operating at somewhat higher voltages. Since the sensor has many advantages over traditional metal oxide gas sensors, there is motivation to further enhance its abilities by adjusting the chemical selectivity to various gas analytes linked to the nature of the deposited nanostructures.

Metal oxide deposition on the PS interface has been shown to increase or decrease the resistance response of the PS sensors to inorganic analyte gases depending on the combination of analyte and decorating metal oxide. The recently implemented Inverse Hard/Soft Acid/Base (IHSAB) model, which predicts the interaction of acidic, basic, and amphoteric gas analytes with nanostructure treated p- and n-type PS sensor interfaces [13], complements the tenants of the HSAB concept [28] and serves as an explanation of this phenomenon.

Figure 9 shows the estimated positions of deposited nanostructures (acids) and analytes (bases) on the IHSAB scale relative to p- or n-type PS. The interaction strength is correlated with the relative acidity and basicity of the reactants, as strong acids react with strong bases and weak acids interact with weak bases, resulting in significant ionic and covalent bonding, respectively. We wish to minimize this bond formation. A nanostructure-treated PS gas sensor can be made to behave in a physisorption/weak chemisorption dominated mode, and the IHSAB concept can be used to explain this behavior. Here,

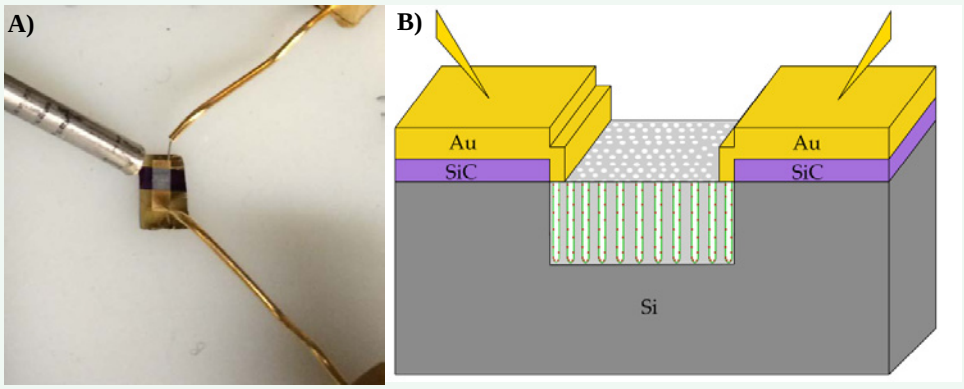

Figure 7 (a) Gas sensor configuration and (b) PS sensor schematic.

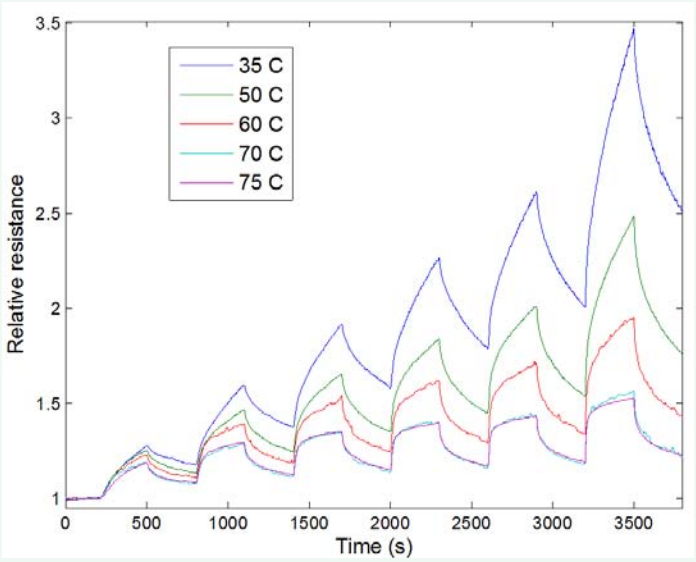

Figure 8 Response of p-type PS sensor to NH_3 at a range of temperatures. The temperature of the sensor is recorded in the figure. The corresponding temperatures of the heat source are 45ºC, 92ºC, 160ºC, 200ºC, and 240ºC.

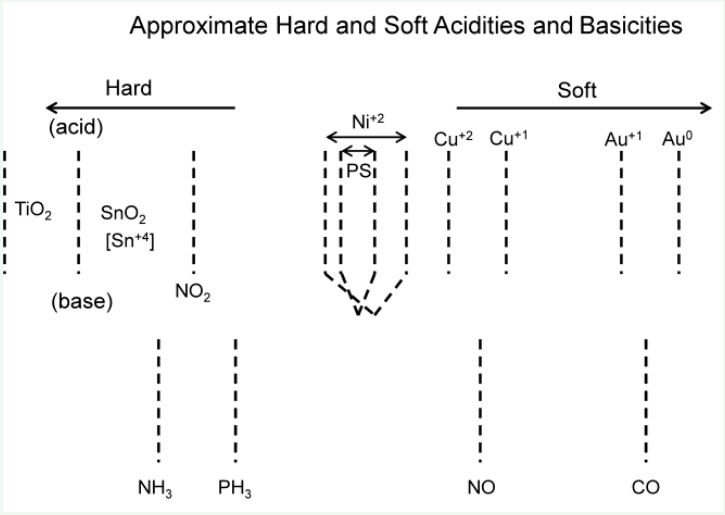

Figure 9 IHSAB scale and estimated hard and soft acidities and bacicities based on resistance changes relative to a p- and n-type PS interface [29].

the physisorption process is found to dominate for primarily strong acid-weak base and weak acid-strong base interactions. The emphasis is to impede bond formation by creating a molecular orbital mismatch. By assessing trends within the IHSAB framework, appropriate selections can be made for the modification of the PS hybrid interface with nanostructured metal/metal oxide deposits to create a range of sensitivities for a number of gases [29]. A weak interaction with minimal chemical bonding occurs if the donor orbital (highest occupied molecular orbital, HOMO) energy is not well matched with the acceptor (lowest occupied molecular orbital, LUMO) energy. As the HOMO (donor)-LUMO (acceptor) energy gap decreases, there will be more charge transfer and a stronger Lewis acid-base interaction. The greater the separation, the greater the orbital mismatch, leading to a greater response of the sensor [29]. As dictated by the IHSAB scale, Au_xO will produce the largest response to NH_3 and TiO_2 and SnO_2 will produce the largest response to CO. The IHSAB principle may, in fact offer an alternate explanation to the observations of Yan et al. [23].

If nanoparticles of TiO_2, a very hard acid, are deposited on an n-type PS sensor, they greatly enhance the response to NH_3, a hard base (Figure 10). The TiO_2 nanostructure shifts the PS interface toward a position much farther away from NH_3, increasing the inverse hard/soft relation and improving the physisorption directed response. Acting as a base, NH_3 contributes electrons to an n-type PS, increasing the number of electrons, the majority charge carriers, corresponding to an increase in conductivity or a decrease in resistance [30].

The IHSAB model guides the choice of metal oxide nanoparticles deposited onto the PS micro-/nanoporous interface to create an array of selectively tuned sensors [29]. The relative change in response to NO and NH_3 for an n-type PS sensor resulting from various nanostructure depositions is summarized in (Table 1), where the change is described by,

$$\Delta = \frac{\Delta R(deposited) / R_0(deposited)}{\Delta R(untreated) / R_0(untreated)}.$$

Table 1: Response change, Δ, due to nanostructure depositions on n-type PS [29].

	TiO_2^*	NiO	Au_xO
NO	-12	4	1.5-2
NH_3	3.5-4	1.5	3

*Recorded signal results as the strong acid TiO_2 attracts electrons from the amphoteric NO radical.

This array has recently been expanded by in-situ modification of the deposited metal oxide nanostructures. The metal oxide nanostructure islands on the PS sensors have been functionalized by triethylamine in a manner similar to the nitridation of TiO_2 described previously [31]. The sensor is then aged for 24 hours in a desiccator before testing, thus allowing unreacted triethlyamine to evaporate. The in-situ modification of the deposited metal oxides changes the reversible interaction with NO, NH_3, and other analytes in accordance with relative shifts on the IHSAB scale giving evidence for the creation of oxynitrides [31,32].

Nitridated NiO shifts toward the soft acid side of the IHSAB scale [32], moving farther away from NH_3. This enhances the hard/soft inverse matching, increasing the response shown in (Figure 11(b)) as manifest by a larger decrease in resistance in the presence of NH_3. In contrast, the NiO treated PS interface moves closer to NO upon nitridation. This enhances the molecular orbital matchup, decreasing the response. This is shown in (Figure 11(a)) as a smaller decrease in resistance in the presence of NO [32].

Sulfur group functionalization is also facilitated on the metal oxide decorated PS interface following a similar deposition process as that applied for nitridation [32]. Exposure to diethyl sulfide and/or ethane or butane thiol now produces a more complex functionalization [32]. Rather than a change in basicity or acidity of the metal oxide/PS interface, the interaction with the gas analytes suggests a change in molecular electronic structure explained by the IHSAB model [32]. The sulfur and nitrogen donate electron density, shifting the metal oxide interface towards the softer acid end of the IHSAB scale (Figure 9). When

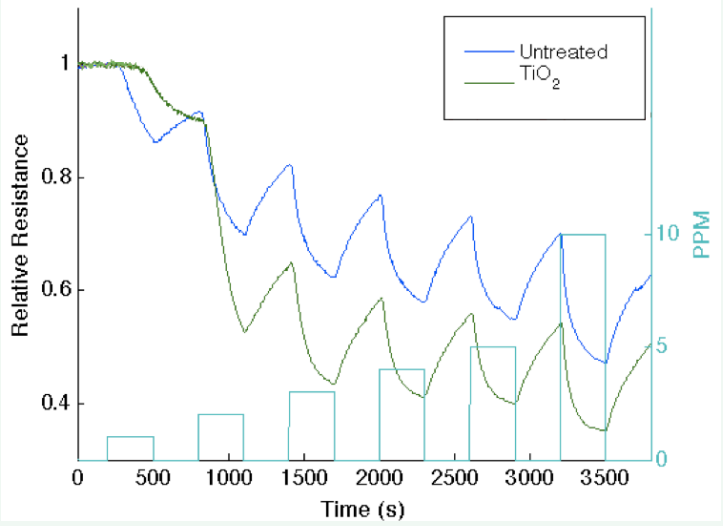

Figure 10 Resistance response to NH_3 of n-type PS and PS/TiO_2 nanostructured sensors at room temperature [30].

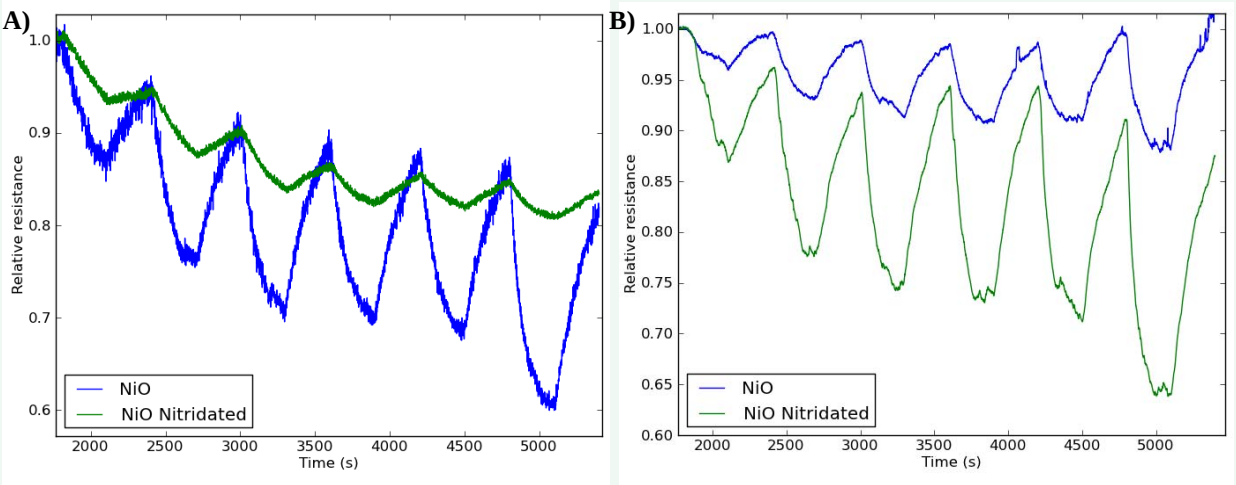

Figure 11 (a) Relative resistance response to NO of NiO and nitridatedNiO treated n-type PS and (b) relative resistance response to NH_3 of NiO and nitridatedNiO treated n-type PS [32].

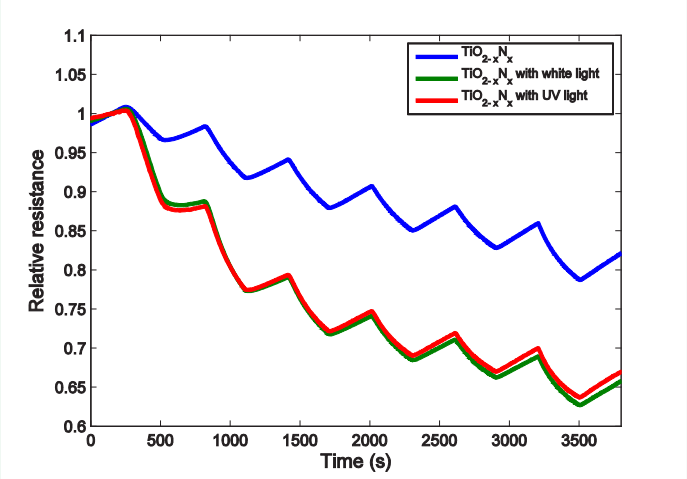

Figure 12 Relative resistance response to NH_3 by $TiO_{2-x}N_x$ decorated n-type PS sensor under UV and white light [30].

applied to TiO_2 decorated PS, the doped TiO_2 moves closer to the fixed position of NH_3 or NO, decreasing the interface/analyte orbital mismatch and the sensor signal decreases. However for NiO, which lies equidistant between NH_3 and NO on the IHSAB scale, a sulfur/nitrogen induced shift to the softer acid side increases the orbital mismatch with NH_3, increasing the sensor response, and decreases the orbital mismatch with NO, decreasing the sensor response (ex: Figure 11). Laminack and Gole encourage the application of these results to form "materials sensitivity matrices" for a given analyte to facilitate sensing gas analyte mixtures [32].

Light enhanced PS gas sensing has also been studied [33,30]. Hui-Qing et al. have measured the change in PS sensor response to NO_2 in the presence of UV radiation [33]. PS at different levels of porosity is formed by electrochemical anodization of p^+-type silicon wafers (0.01-0.012Ω-cm) in 1:1 HF and ethanol with current densities of 40 mA/cm^2, 60 mA/cm^2, and 80 mA/cm^2. The porosities, measured by the gravimetric method, were 65.2%, 71.1%, and 76.8% respectively. To measure the change in response to NO_2, a UV lamp is introduced in the enclosed testing chamber. UV radiation increases the relative resistance change in the presence of UV radiation and they observe the greatest change in sensor response for the PS with the highest porosity. Hui-Qing et al. suggest that this is due to the large number of photo-generated electrons and holes adding to the charge carriers of the p^+-type PS facilitating the reduction and oxidation chemistry of the analyte and PS sensor interface [33].

With the high cost and accessibility of UV photons, in combination with studies of the effects of metal oxide deposition and in-situ nitridation, Laminack and Gole take advantage of the visible-light absorbing spectrum of $TiO2_{-x}N_x$ [30]. TiO_2 and $TiO_{2-x}N_x$ are fractionally deposited to porous silicon, fabricated from n-type silicon wafers as described previously [13]. The metal oxide/PS and nitridated metal oxide/PS sensors are tested in response to NH_3 and NO_2. As a base, NH_3 donates electrons to the n-type PS, increasing the majority charge carriers, thus decreasing

the resistance. Both white light and UV light were shown to have no effect on the resistance response of the PS sensor prior to metal oxide deposition. Upon deposition of the hard acid TiO_2, the interface is shifted to the hard acid end of the IHSAB scale and the response to NH_3 increases. After in-situ conversion to $TiO_{2-x}N_x$, the interface obtains a more basic character reducing the capture of the NH_3 donated electrons and the sensor response. In the presence of UV light, the response for the TiO_2 decorated PS sensor improves by over 100% whereas the visible light has no effect. In contrast, as shown in (Figure 12), the response to NH_3 is increased in the $TiO_{2-x}N_x$ modified PS sensor for both UV and white light [30]. Laminack and Gole explain that the UV and white light excitation causes the $TiO_{2-x}N_x$ to become more acidic, enhancing the electron withdrawing power and thus increasing the sensor response [30].

DISCUSSION AND CONCLUSION

Porous silicon (PS) gas sensors have recently attracted much attention and study. The advantages of PS as a sensor include high surface area, facile circuit integration, optical and chemical response to gas analytes, and ease of modification. Organic vapors (ethanol, DMF, acetone, decane, methylamine, toluene, hexane, methanol, propanol, butanol) and inorganic vapors (CO_2, NH_3, NO_x, CO, SO_2 and PH_3) have been detected. Inorganic vapors are detected at significantly lower concentrations than that of organics. Selectivity is enhanced via comparing multiple aspects of optical and conductance measurements and by increasing the sensitivity to individual gas analytes. Sensitivity is improved with integrated fiber optic design, polypyrrole, and metal oxide (SnO_2, NiO, Fe_2O_3, CoO, ZnO, WO_3, Au_xO, TiO_2) deposition. Nitrogen and sulfur functionalization extend the sensitivity array. Visible and UV light also have been shown to enhance PS sensitivity. The development of a sensitive and selective array of PS gas sensors is studied to make possible the differentiation between gas analyte responses. Therefore, modified PS gas sensors provide a promising platform for further study.

ACKNOWLEDGEMENTS

The authors acknowledge helpful discussions with Kent Barefield, Mark White, and Dave Dixon.

REFERENCES

1. Korotcenkov G, Cho B. Porous Semiconductors: Advanced Material for Gas Sensor Applications. Critical Reviews in Solid State and Materials Sciences. 2010; 35-1: 1-37.
2. Smith R, Collins S. Porous silicon formation mechanisms. J Apple Phys. 1992; 71-8: R1-R22.
3. Eranna C, Joshi B, Runthala D, Gupta R. Oxide Materials for Development of Integrated Gas Sensors – A Comprehensive Review. Critical Reviews in Solid State and Materials Sciences. 2004; 29: 111-188.
4. Ozdemir S, Gole J. The potential of porous silicon gas sensors. Current Opinion in Solid State and Materials Science. 2007; 11: 92-100.
5. Zeidler MR, Kleerup EC, Tashkin DP. Exhaled nitric oxide in the assessment of asthma. Curr Opin Pulm Med. 2004; 10: 31-36.
6. Gerry Teague, private communication.
7. Gomzi M. Indoor air and respiratory health in preadolescent children. Atmospheric Environment. 1999; 33: 4091-4086.
8. Berck B. Sorption of phosphine by cereal products. J Agric Food Chem. 1968; 16: 419-425.
9. Burgess J L, Burgess J. Phosphine exposure from a methamphetamine laboratory investigation. J Toxicol Clin Toxicol. 2001; 39: 165-168.
10. King B, Ruminski A, Snyder J, Sailor M. Optical-Fiber-Mounted Porous Silicon Photonic Crystals for Sensing Organic Vapor Breakthrough in Activated Carbon. Adv Mater. 2007; 19: 4530-4534.
11. Uhde E, Salthammer T. Impact of reaction products from building materials and furnishings on indoor air quality – A review of recent advances in indoor chemistry. Atmospheric Environment. 2007; 21: 3111-3128.
12. Jalkanen T, Tuura J, Mäkilä E, Salonen J. Electro-optical porous silicon gas sensor with enhanced selectivity. Sensors and Actuators B: Chemical. 2010; 147-1: 100-104.
13. Gole J L, Goude E C, Laminack W. Nanostructure-driven analyte-interface electron transduction: a general approach to sensor and microreactor design. ChemPhysChem. 2012; 13: 549-561.
14. Karacali T, Hasar H, Ozbeck I, Oral A, Efeoglu H. Novel Design of Porous Silicon Based Sensor for Reliable and Feasible Chemical Gas Vapor Detection. Journal of Lightwave Technology. 2013; 31: 295-305.
15. Jalkanen T, Torres-Costa V, Salonen J, Björkqvist M, Mäkilä E, Martínez-Duart J M, et al. Optical gas sensing properties of thermally hydrocarbonized porous silicon Bragg reflectors. Opt Express. 2009; 17: 5446-5456.
16. Nguyen M H, Tsai H J, Wu J K, Wu Y S, Lee M C, Tseng F G. Cascaded nano-porous silicon for high sensitive biosensing and functional group distinguishing by Mid-IR spectra. Biosens Bioelectron. 2013; 47: 80-85.
17. Moshnikov V, Gracheva I, Lenshin A, Spivak Y, Anchikov M, Kuznetov V, et al. Porous silicon with embedded metal oxides for gas sensing applications. Journal of Non-Crystalline Solids. 2012; 358: 590-595.
18. Liyanage C N, Blackwood D J. Functionalization of a porous silicon impedance sensor. Thin Solid Films. 2014; 550: 677-682.
19. Hu J, Wu P, Deng D, Jiang X, Hou X, Lv Y. An optical humidity sensor based on CdTenanocrystals modified porous silicon. Microchemical Journal. 2013; 108: 100-105.
20. Cho S, Lee K, Kim J, Kim D. Rugate-structured free-standing porous silicon-based fiber-optic sensor for the simultaneous detection of pressure and organic gases. Sensors and Actuators B: Chemical. 2013; 183: 428-433.
21. Gole J L, Ozdemir S. Nanostructure-directed physisorption vs chemisorption at semiconductor interfaces: the inverse of the HSAB concept. ChemPhysChem. 2010; 11: 2573-2581.
22. Tebizi-Tighilt F, Zane F, Belhaneche-Bensemra N, Belhousse S, Sam S, Gabouze N. Electrochemical gas sensors based on polypyrrole-porous silicon. Applied Surface Science. 2013; 269: 180-183.
23. Yan D, Hu M, Li S, Liang J, Wu Y, Ma S. Electrochemical deposition of ZnO nanostructures onto porous silicon and their enhanced gas sensing to NO_2 at room temperature. ElectrochimicaActa. 2014; 115: 297-305.
24. Ma S, Hu M, Zeng P, Li M, Yan W, Li C. Synthesis of tungsten oxide nanowires/porous silicon composites and their application in NO_2 sensors. Materials Letters. 2013; 112: 12-15.
25. Wu Y, Hu M, Qin Y, Wei X, Ma S, Yan D. Enhanced response characteristics of p-porous silicon (substrate)/p-TeO_2 (nanowires) sensor for NO_2 detection. Sensors and Actuators B: Chemical. 2014; 196: 181-188
26. Laminack W, Pouse N, Gole J L. Dynamic Interaction of NO_2 with

a Nanostructure Modified Porous Silicon Matrix: Acidity, Sensor Response, and the Competition for Donor Level Electrons. ECS Journal of Solid State Science and Technology. 2012; 1: Q25-Q34.

27. Ozdemir S, Gole J. Porous Silicon Gas Sensors for Room Temperature Detection of Ammonia and Phosphine. ECS Transactions. 2008; 16: 379-385.

28. Pearson R G. Hard and Soft Acids and Bases – The Evolution of A Chemical Concept. Coord Chem Rev. 1990; 100: 403-425.

29. Gole J, Laminack W. Nanostructure Modified Porous Interfaces for Enhanced Sensing and Directed Microcatalysis. ECS Transactions. 2013; 50: 237-246.

30. Laminack W, Gole J. Light Enhanced Transduction and Amplified Sensing at a Nanostructure Modified Semiconductor Interface. Advanced Functional Materials. 2013; 23: 5916-5924.

31. Gole J L, Stout J, Burda C, Lou Y, Chen X. Highly Efficient Formation of Visible Light Tunable TiO_2-xN_x Photocatalysts and Their Transformation at the Nanoscale. J Phys Chem. 2004; 108: 1230-1240.

32. Gole J L, Laminack W. Nanostructure-directed chemical sensing: The IHSAB principle and the dynamics of acid/base-interface interaction. Beilstein J Nanotechnol. 2013; 4: 20-31.

33. Hui-Qing C, Ming H, Jing Z, Wei-Dan W. The light-enhanced NO_2 sensing properties of porous silicon gas sensors at room temperature. Chin Phys B. 2012; 21: 1-5.

Cite this article

Baker C, Gole JL (2014) Interface Modifications of Porous Silicon for Chemical Sensor Applications. JSM Nanotechnol Nanomed 2(1): 1021.